Applied Catalysis B: Environmental 125 (2012) 390–397

Contents lists available at SciVerse ScienceDirect

Applied Catalysis B: Environmental

journal homepage: www.elsevier.com/locate/apcatb

Synthesis and characterization Pt nanocatalysts on tungsten based supports for oxygen reduction reaction

N.R. Elezovic[a,*,1], B.M. Babic[b], P. Ercius[c], V.R. Radmilovic[d], Lj.M. Vracar[d], N.V. Krstajic[d]

[a] Institute for Multidisciplinary Research, University of Belgrade, Kneza Viseslava 1, Belgrade, Serbia
[b] Vinca Institute of Nuclear Sciences, University of Belgrade, Serbia
[c] National Center for Electron Microscopy, LBNL University of California, Berkeley, CA, USA
[d] Faculty of Technology and Metallurgy, University of Belgrade, Belgrade, Serbia

ARTICLE INFO

Article history:
Received 19 March 2012
Received in revised form 8 June 2012
Accepted 12 June 2012
Available online 21 June 2012

Keywords:
Tungsten based support
Pt/WC catalyst
Oxygen reduction reaction
Acid solution

ABSTRACT

Platinum nanocatalysts on two tungsten based supports have been synthesized and characterized as catalysts for oxygen reduction reaction in 0.5 mol dm^{-3} $HClO_4$ solution, at 25 °C. Tungsten based support assigned WCctabr has been synthesized by polycondensation of resorcinol and formaldehyde in the presence of CTABr surfactant. Support assigned WC_{WO_3} was synthesized from resorcinol/formaldehyde gel, using WO_3 nanoparticles as starting material. Supporting materials have been characterized by BET (Brunauer, Emmett and Teller) technique and determined values of surface area were 80 m^2 g^{-1} for WCctabr and 175 m^2 g^{-1} for WC_{WO_3}.

Platinum nanocatalysts (10% Pt) at tungsten based supports have been prepared by borohydride reduction method. Both synthesized supports and catalysts have been characterized by X-ray diffraction (XRD), transmission electron microscopy (TEM) and electron energy loss spectroscopy (EELS) techniques. Cyclic voltammetry was applied for determination of electrochemically active surface area (40 m^2 g^{-1} for Pt/WC_{WO_3} and 55 m^2 g^{-1} for Pt/WCctabr).

Oxygen reduction reaction has been studied by cyclic voltammetry and linear sweep voltammetry at rotating disc electrode (RDE). These catalysts exhibited better catalytic activity, expressed in terms of kinetic current density per real surface area at the constant potential and better stability, in comparison with Pt/C catalyst, as well as with already reported catalytic activity values for Pt catalysts on tungsten based supports.

1. Introduction

Proton exchange membrane fuel cells (PEMFCs) are promising future power sources. In spite of the researchers' efforts during last few decades, many questions in this field still remain unresolved. The cell performance is significantly influenced by oxygen reduction reaction, owing slow oxygen reduction kinetics and much higher overpotential, compared to fast anodic hydrogen oxidation. Stability, performance and durability are the major issues for oxygen reduction reaction catalysts and key points of this class fuel cell's limits [1].

Platinum based catalysts exhibit the best catalytic activity for oxygen reduction reaction. On the contrary, platinum as high cost material diminishes possibility of practical application. In order to decrease amount of platinum and lower costs, platinum nanoparticles deposited at high surface area carbon supports have been investigated as promising materials for PEMFCs applications [2–6]. The crucial role of catalyst support has been recognized. Supporting material should be combination of high conductivity and corrosion stability, to increase life time and durability of fuel cell. PEMFCs in, for instance automotive applications, are expected to experience many start-up/shutdown cycles during operating time [7]. After shutdown, the hydrogen will be removed from the stack. During next start up, when hydrogen is reintroduced, electrode potential could exceed 1.4 V for short period of time. The catalyst support must be able to survive these high potentials in order to provide necessary durability [8]. According to Mathias et al. [7], currently used carbon based supports (Vulcan XC-72R and Ketjen) do not meet automotive durability requirements. Carbon corrosion, that could proceed either during recharge of the fuel cell, at the air electrode, or at start/stop conditions of a simple fuel cell [9] is one of the main factors that could decrease life time of PEMFCs. In the presence of water, carbon can also be consumed in heterogeneous reaction: $C + H_2O \rightarrow H_2 + CO$ [10], especially in the presence of

* Corresponding author.
E-mail address: nelezovic@tmf.bg.ac.rs (N.R. Elezovic).
[1] ISE member.

0926-3373/$ – see front matter © 2012 Elsevier B.V. All rights reserved.
http://dx.doi.org/10.1016/j.apcatb.2012.06.008

platinum which catalyzes this reaction. Moreover, the reaction product CO might poison the Pt catalyst.

Above mentioned disadvantages of carbon based supports imply need for new supporting materials, in order to prevent damage of Pt nanocatalysts, enhance the durability and reliability and to reduce the total lifetime costs for PEMFC, as well.

Tungsten carbide is known as the best conductive (10^5 S cm^{-1} at 20 °C) among interstitial carbides. It was investigated as a potential electrocatalyst for PEMFCs owing its platinum like catalyst behavior [11]. Tungsten carbide, as low cost alternative to bulk precious metal catalysts, is an excellent candidate support material for Pt monolayer, leading to good adhesion and utilizing the lowest possible Pt loading [12]. Electrochemical stability of tungsten and tungsten carbide over wide pH and potential ranges have been studied and both materials showed promise as an anode, while operating within the region of passivation, and as a cathode, across the entire pH range [13]. Tungsten carbide could be prepared by many methods, but the key issue in the synthesis is the difficulty to produce tungsten carbide with high surface area, because of temperature induced sintering [14]. Pt based catalyst on tungsten carbide dispersed on high surface area carbon has been studied and showed remarkable activity for oxygen reduction and hydrogen oxidation reaction [15]. Potential suitability of WC as a PEMFCs catalyst support has been investigated by Chhina et al. [8] and significantly higher electrochemical stability of this support comparing to Vulcan XC-72R in accelerated oxidation cycling tests has been reported. Single cell tests using Pt/W_xC_y catalyst were performed and higher oxidation resistance in comparison with Pt/C catalyst was observed [16]. Pt nanoparticles supported on mesoporous carbon, modified with tungsten carbide exhibited enhanced thermal and electrochemical stability [14]. High surface area tungsten carbide microsphere (TCMSs) have been successfully synthesized by hydrothermal method and characterized as Pt catalyst support [17]. Nanosized WC, synthesized by intermittent microwave heating methods was used as support for Pt nanoparticles, promising results for alcohol oxidation and oxygen reduction reactions have been reported [18]. Jeon et al. [19] suggested Pt/WC/C catalyst for both anode and cathode applications. In review paper dealing with tungsten based materials for fuel cells applications, by Antolini and Gonzalez [20], W_2C was reported as the most promising co-catalyst in Pt/W_2C for oxygen reduction reaction, while WO_3 and W_xC as stable carbon-alternative catalyst supports were suggested. Oxygen reduction on tungsten promoted Pt/C (Pt-W_2C/C) composite catalyst, prepared by intermittent microwave irradiation method was significantly enhanced, probably due to the synergetic effect between nanocrystalline tungsten carbide and Pt [21]. Nanostructured Pt-WC_x/carbon nanotube catalyst (CNTs), prepared by microwave-assisted thermolytic molecular precursor method, was characterized as efficient for oxygen reduction reaction [22]. The unique electrocatalytic properties of the Pt-WC_x/CNTs catalyst were attributed to synergetic effect between Pt, WC_x and CNTs. Tungsten carbide modified high surface area carbon (commercial Ketjen black) support-WC/KB, was synthesized by temperature programmed reaction method and Pt catalyst on WC/KB has been tested in fuel cell conditions [23]. Similar or slightly better ORR catalytic activity of Pt/WC/KB catalyst, compared to Pt/KB, has been reported [23]. The Pt activity loss rate of Pt/WC/KB was slightly lower than that of Pt/KB in the liquid cell testing due to the larger Pt particle size or some interaction between Pt and WC [23]. An attempt to use atomic layer deposition (ALD) as a synthesis method to deposit monolayer of Pt onto WC substrate for applications as electrocatalyst for oxygen reduction reaction was made. It was found that Pt deposition onto WC followed island growth mechanism, so monolayer has not been obtained [24].

In this work tungsten based supports (assigned as WCctabr and WC_{WO_3}) have been synthesized by two novel different synthesis methods. Platinum nanocatalysts on these supports were synthesized by borohydride reduction method. Catalysts were tested for ORR in 0.5 mol dm^{-3} $HClO_4$ and better catalytic activity was obtained, in comparison with Pt/C, as well as with already reported catalytic activity values for Pt catalysts on tungsten based supports.

The best stability, after repetitive cyclic voltammetry tests performed, exhibited Pt/WC_{WO_3} catalyst.

2. Experimental

2.1. Synthesis of WCctabr support

Support assigned as WCctabr was prepared by polycondensation of resorcinol and formaldehyde in the presence of cetyltrimethylammoniumbromide (CTABr) surfactant, using modified method proposed by Ganesan et al. [25]. 6.14 g CTABr was dissolved in 20 ml of distilled water. The solution containing 4.073 g of ammonium metatungstate salt (AMT), 1.13 g of resorcinol and 1.7 ml of formaldehyde in 10 ml H_2O was added to the CTABr solution. Solution was decanted, sealed and placed for 3 days at 25 °C, 1 day at 50 °C and 3 days at 85 °C. Resorcinol/formaldehyde gel was immersed in a 10-times volume of t-butanol for 1 day. After that time, rinsing with t-butanol was repeated twice.

The sample was pre-frozen at −30 °C for 24 h. After that, it was dried frozen for 20 h at the pressure of 4 mbar. The red colored cryogel was treated in Ar flow atmosphere, at 900 °C for 1 h.

2.2. Synthesis of WC_{WO_3} support

WO_3 nanoparticles were obtained by dissolution of 5 g W-powder in 50 ml of 30% H_2O_2 solution, 5 ml 2-propanol and 10 ml H_2O. Prepared WO_3 particles were separated by centrifugation and dried at 80 °C. Two grams of formaldehyde and 1.32 g resorcinol were dissolved in 9.6 ml H_2O, with addition of 0.0132 g Na_2CO_3 and 2.46 g WO_3 powder. This suspension was vigorously stirred at 50 °C, for 1 day, and at 85 °C, for 3 days. The obtained gel was freeze dried for 12 h. Prepared solid was treated in Ar flow, at 900 °C, for 1 h.

2.3. Preparation of tungsten carbide supported Pt catalysts

WC supported Pt (10 wt.%) nanocatalysts were prepared by borohydride reduction method [26]. The main steps of this synthesis were following: appropriate amount of H_2PtCl_6 was dissolved in D.I. water. WC support was dispersed in D.I. water and then mixed by adding platinum salt solution under constant stirring. The mixture of platinum salt and support was reduced by excess of sodium borohydride solution. Prepared precipitate was washed with water (18 MΩ) and then dried at 80 °C.

The Vulcan/Pt catalyst, with specific surface area of 92 m^2 g^{-1}, used as benchmark, was synthesized by modified ethylene glycol method on a commercial VulcanXC-72 support. The preparation procedure was fully described in Ref. [27].

2.4. Physical characterization of the supports and catalysts

Specific surface areas, S_{BET}, of the supports were determined by measuring a volume of nitrogen adsorbed onto a specific mass of each sample, as a function of gas pressure, applying gravimetric Mc Bain method.

The support powders were also characterized by X-ray diffraction (XRD) technique on a Siemens D500 X-ray diffractometer using Cu Kα radiation with a Ni filter. The 2θ angular regions between 5° and 80° were explored at a scan rate of 0.02°/s with the angular resolution of 0.02° for all XRD tests.

High angle annular dark field scanning transmission electron microscopy (HAADF-STEM), bright field transmission electron microscopy (BF-TEM), and electron energy loss spectroscopy (EELS) techniques (National Center for Electron Microscopy NCEM-Lawrence Berkeley National Laboratory, Berkeley, USA) for surface characterization of the supports and catalyst materials have been applied.

2.5. Electrochemical characterization

Electrochemical measurements were performed in a conventional three-compartment glass cell, at the temperature of 25 °C, in 0.5 mol dm^{-3} $HClO_4$ high-purity solution (Spectrograde, Merck), prepared in 18.2 MΩ pure water. The counter electrode was a platinum sheet of 5 cm^2 geometric area. A platinum plated Pt reversible hydrogen electrode (RHE) in the same solution and at the same temperature was used as the reference electrode.

The working electrode was gold rotating disk (diameter 5 mm). The ink was suspension of catalyst in ethanol and Nafion solution (5 wt.% Aldrich solution). It was first ultrasonically dispersed for 30 min. Aliquot of ink was transferred on the gold electrode and dried at 80 °C for 10 min to obtain thin film. The Pt loading was 8 μg of Pt. Mayrhofer et al. [28] suggested that 42 $\mu g_{Pt}\ cm^{-2}_{disc}$ is optimal loading for the fuel cell cathode. Namely, due to low Pt loading RDE could not be completely and homogenously covered. On the contrary, too high Pt loading implies that mass transport characteristics of the RDE are no longer satisfied.

Electrochemical measurements have been performed using potentiostat/galvanostat PAR Model 273.

3. Results and discussion

3.1. BET and XRD analysis

Nitrogen adsorption isotherms for WC_{WO_3} and WCctabr supports have been presented in Fig. 1a and b, as well as corresponding pore size distributions (insets in Fig. 1a and b). It could be seen that both supports are mesoporous materials. Determined values of specific BET surface area for WC_{WO_3} and WCctabr supports were 175 m^2 g^{-1} and 80 m^2 g^{-1}, respectively. Pore size distribution diagrams showed the sharp peaks, with the maximum pore size radius between 2 and 3 nm for WC_{WO_3} and 1 and 2 nm for WCctabr support.

Fig. 2a–d represents typical XRD patterns for WC_{WO_3} support, WCctabr support, Pt/WC_{WO_3} and Pt/WCctabr catalyst, respectively. Fig. 2a shows the XRD pattern of the WC_{WO_3} support. XRD pattern clearly shows existence of tungsten. The observed peaks correspond to the following facets of metallic W: (1 1 0) for 2θ-40.26, (2 0 0) for 2θ-58.27 and (2 1 1) for 2θ-73.19. These results indicate that tungsten oxide was converted either to tungsten, or to the mixture of different carbides, in the quantity of few monolayers, and because of that they could not be detected by XRD technique, or even that the formed carbides do not have crystalline structure.

Fig. 2b represents XRD pattern of WCctabr support. The diffraction peaks at 40.26°, 58.27° 73.19° and 87.017° correspond to metallic W. The peak at 2θ = 35.98° corresponds to (1 0 0) facet of WC.

To make clear the surface state of the supports, these materials have been characterized by STEM and EELS techniques.

The XRD patterns for Pt nanocatalysts show typically peaks arising from the Pt nanoparticles (fcc structure; JCPDS card no. 04-0802). Fig. 2c and d represents XRD patterns of Pt/WC_{WO_3} and Pt/WCctabr catalyst, respectively. Broad diffraction peaks belonging to Pt overlap with the corresponding peaks of the support. The presented broad peaks indicated small Pt particle size, as it

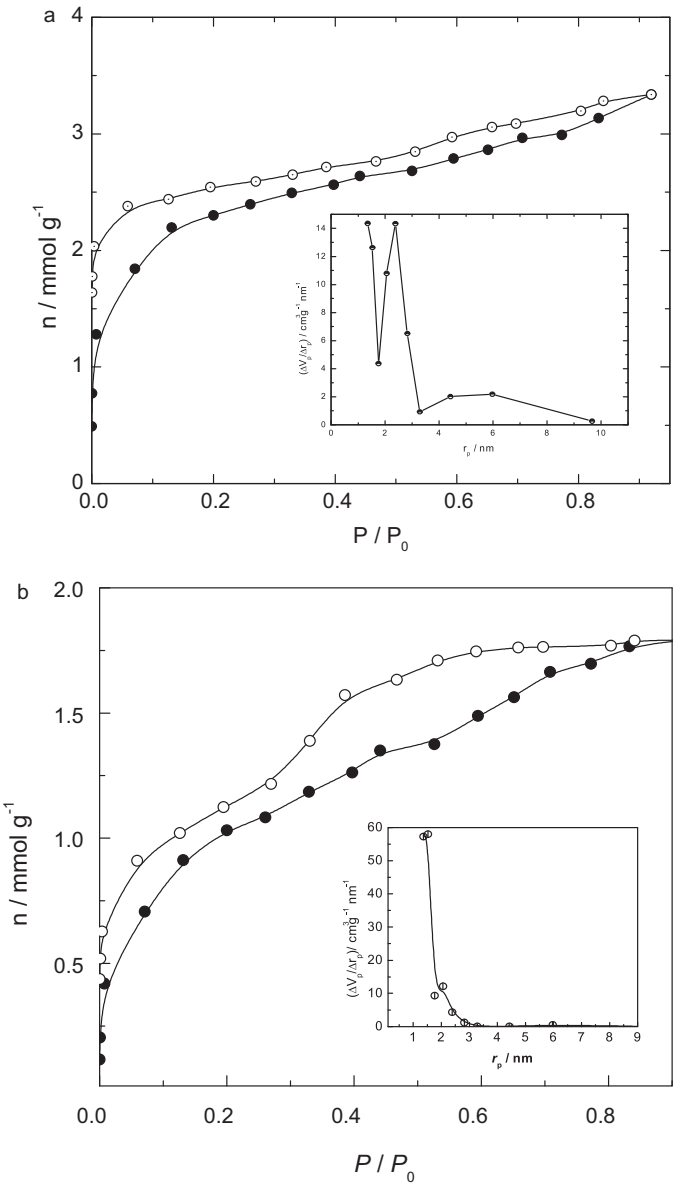

Fig. 1. Nitrogen adsorption isotherm for WC_{WO_3} support (a) and WCctabr support (b). Insets: corresponding pore size distributions.

was confirmed by TEM technique. Namely, transmission electron microscopy showed very small Pt particles, about 2 nm in size, even the clusters of Pt atoms (Section 3.2). Other possible explanation could be tungsten based supports transformation into amorphous hydride structure during Pt deposition, since H_2 is released during borohydride reduction.

3.2. STEM analysis

Fig. 3a presents low magnification TEM image of WC_{WO_3} support. It could be seen presence of two W particle sizes, larger above 5 nm in diameter, and smaller below 2 nm in diameter. Two different particles types could be observed: white brilliant particles correspond to WO_3, until gray belong to tungsten. High resolution TEM micrograph of WC_{WO_3} support clearly indicates presence of WC islands on W particle (Fig. 3b).

High angle annular dark field (HAADF) STEM and STEM-BF (bright field) micrographs of Pt/WC_{WO_3} are presented in Fig. 4a–c. Typical bimodal size distribution of Pt particles is observed: large

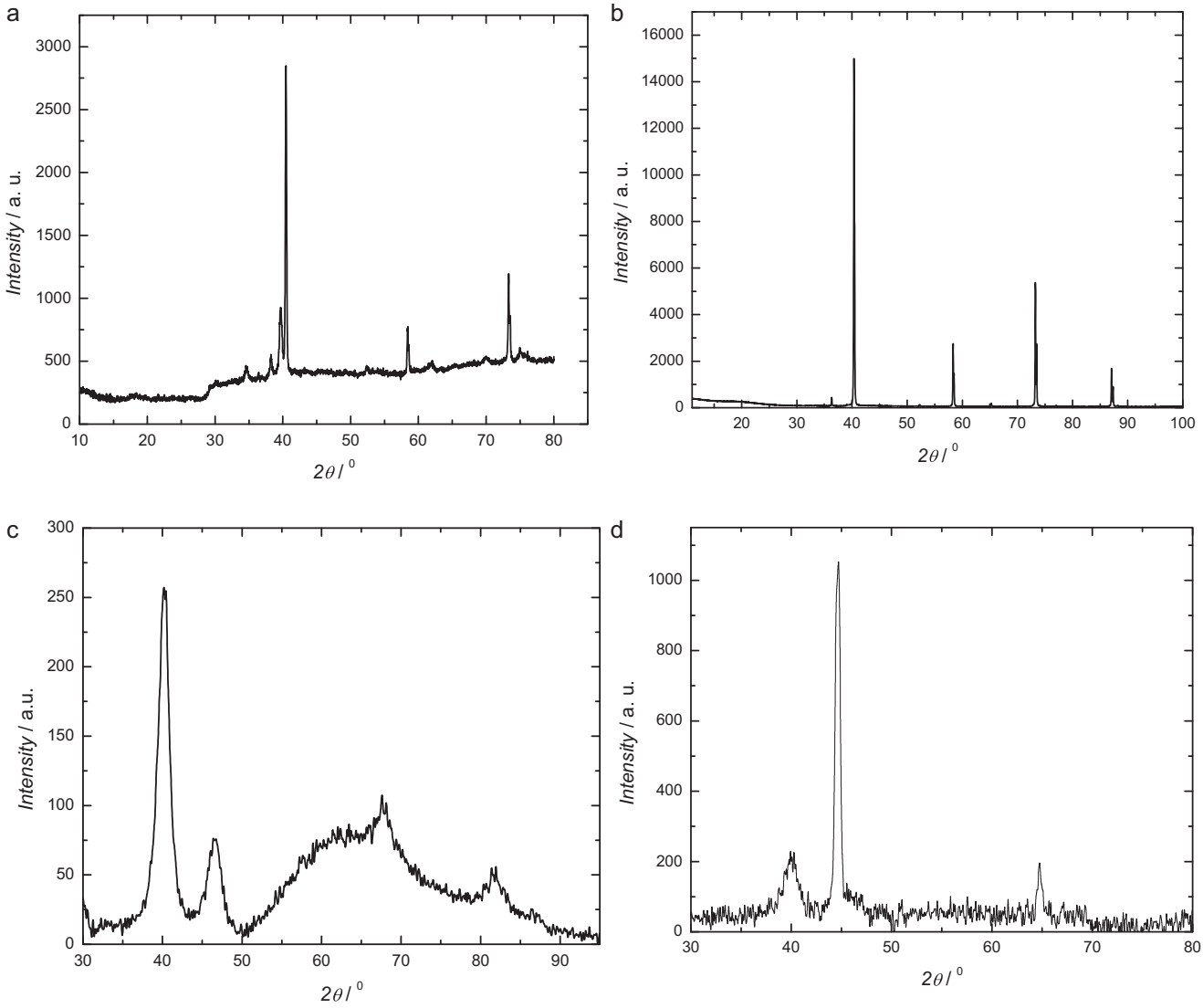

Fig. 2. XRD patterns for WC_{WO_3} support (a), WCctabr support (b), Pt/WC_{WO_3} catalyst (c) and Pt/WCctabr catalyst (d).

of the size between 5 and 10 nm, and small of the size less than 2 nm (Fig. 4a). A lot of clusters of individual Pt atoms on support were also observed. Indication that Pt particle could be nucleating on W particle is illustrated in Fig. 4b and c. Namely, the presented bright field STEM image (Fig. 4c) clearly indicated one dimensional lattice belonging to the Pt (1 1 1) and tungsten particles oriented to 1 0 0 zone axis (upper and lower black square at Fig. 4c).

BF-TEM image of WCctabr support is presented in Fig. 5, showing core–shell structure, containing W core and WC shell about 2–5 nm of thickness. EDS analysis confirmed that shell was mixture of tungsten oxide and tungsten carbide. EELS have been performed as complementary technique to EDS spectroscopy, to confirm core–shell structure.

Fig. 6a represents TEM micrograph of Pt/WCctabr catalyst. Homogenous platinum particle distribution over the support is observed. High resolution electron microscopy results with corresponding HREM spectrum are presented in Fig. 6b. Peaks corresponding to Pt and W could be observed. White size circle indicates size and beam position.

3.3. Electrochemical characterization

Cyclic voltammetry results recorded in the potential range from 0.03 V to 1.4 V vs RHE in 0.5 mol dm^{-3} $HClO_4$ at Pt/WC_{WO_3}, Pt/WCctabr and Pt/C have been presented in Fig. 7, Fig. 8 and Fig. 9, respectively. Electrochemically active surface area of each catalyst

Table 1
Specific and mass activities for different Pt catalysts on tungsten based supports and Pt/C catalyst at the constant potential.

Catalyst	Electrochemically active surface area (m^2 g^{-1} Pt)	Mass activity (mA/mg Pt) at E = 0.85 V (RHE)	Specific activity (μA cm^{-2} Pt) at E = 0.85 V (RHE)
Pt/C	92	243	265
Pt/WCctabr	55	287	523
Pt/WC_{WO_3}	40	218	547
Pt-W_2C/C [15]	–	–	300

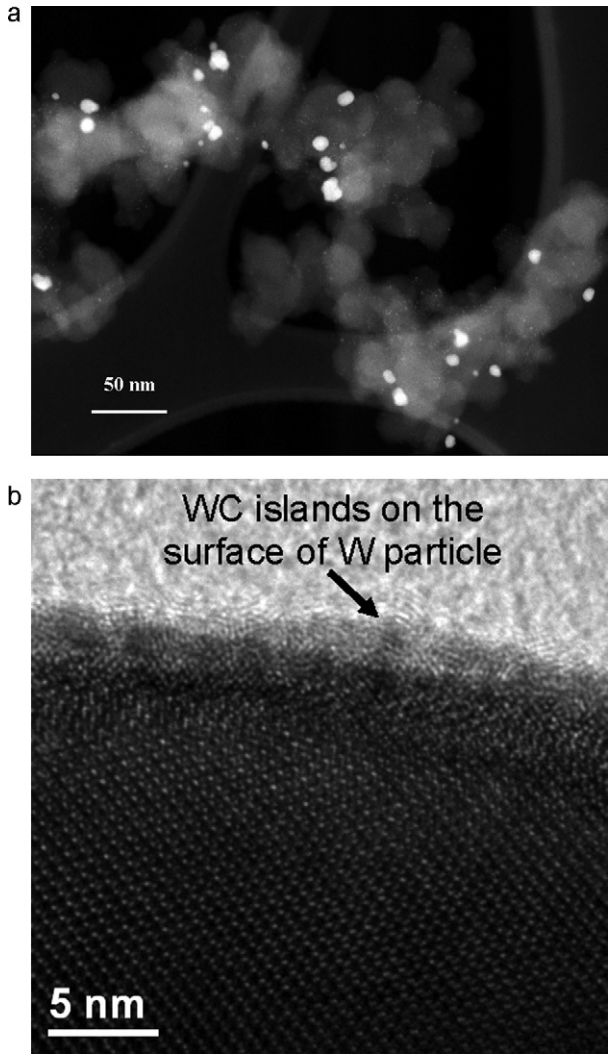

Fig. 3. (a) Low magnification TEM image of WC_{WO_3} support, (b) HRTEM micrograph of WC_{WO_3} support-indicating WC islands on W particles.

has been estimated from the charge obtained by integration of anodic part of cyclic voltammogram in the hydrogen underpotential deposition region, taking into account value of 210 μC cm^{-2} for full platinum monolayer. Determined values are presented in Table 1. The electrochemical stability of all these catalysts was tested by repetitive cycling in the same potential range. It is well known that carbon based supports undergo corrosion at anodic potential about 1.4 V vs RHE, causing degradation of the catalysts and decreasing its durability and life time. Degradation of the support could be experimentally confirmed by repetitive cycling in this potential range. Namely, electrochemically active surface area, determined by integration of obtained cyclic voltammograms in the potential range where underpotential deposition of hydrogen takes place, should be reduced. Presented results clearly proved the differences between the catalysts, with the best stability of Pt/WC_{WO_3} (Figs. 7–9). Namely, after 100 cycles Pt/C catalyst exhibited significant loss of electrochemically active surface area (Fig. 9). Similar behavior have been reported by Chhina et al. [8,29] – they found that electrochemical activity of the Pt/WC remained nearly constant after 100 oxidation cycles, while the activity of Pt/C was almost completely lost after only 20 cycles. On the other hand, electrochemically active surface area of Pt for Pt/WC_{WO_3} was almost the same after 100 cycles (Fig. 7).

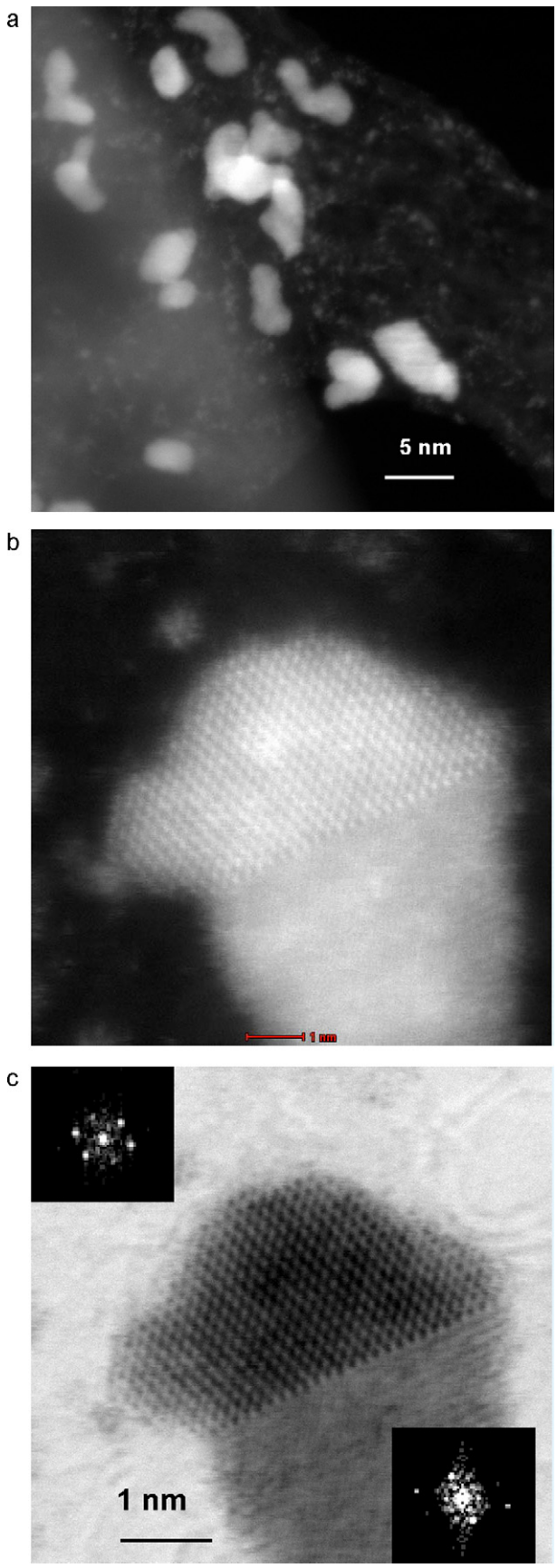

Fig. 4. (a) TEM micrograph of Pt/WC_{WO_3} catalyst, showing bimodal particle size distribution; (b) and (c) HRTEM results for Pt/WC_{WO_3} catalyst, indicating nucleation of Pt at W particles.

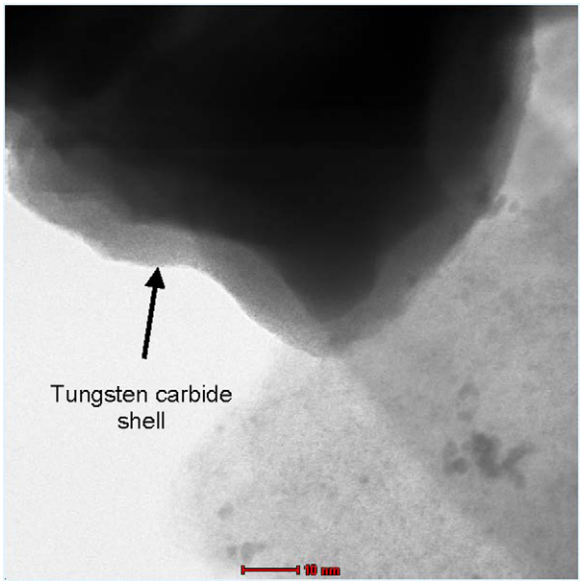

Fig. 5. High resolution TEM micrograph of WCctabr support.

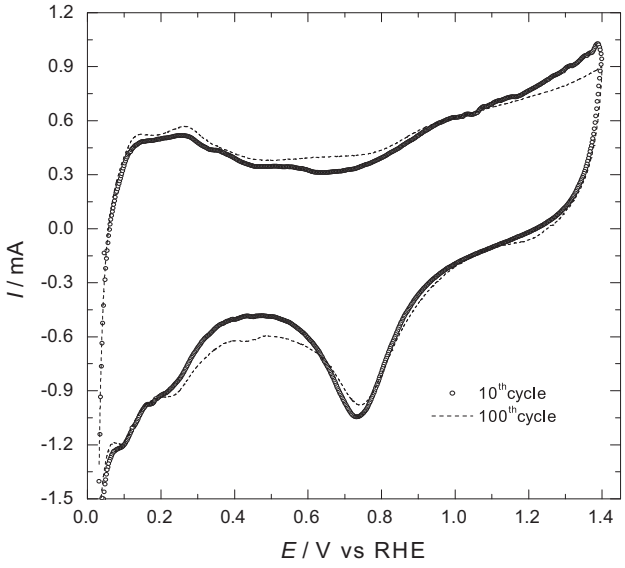

Fig. 7. Cyclic voltammetry results obtained after 10 and 100 cycles, at Pt/WC_{WO_3} RDE in 0.5 mol dm^{-3} $HClO_4$, at 25 °C with sweep rate of 100 mV s^{-1}.

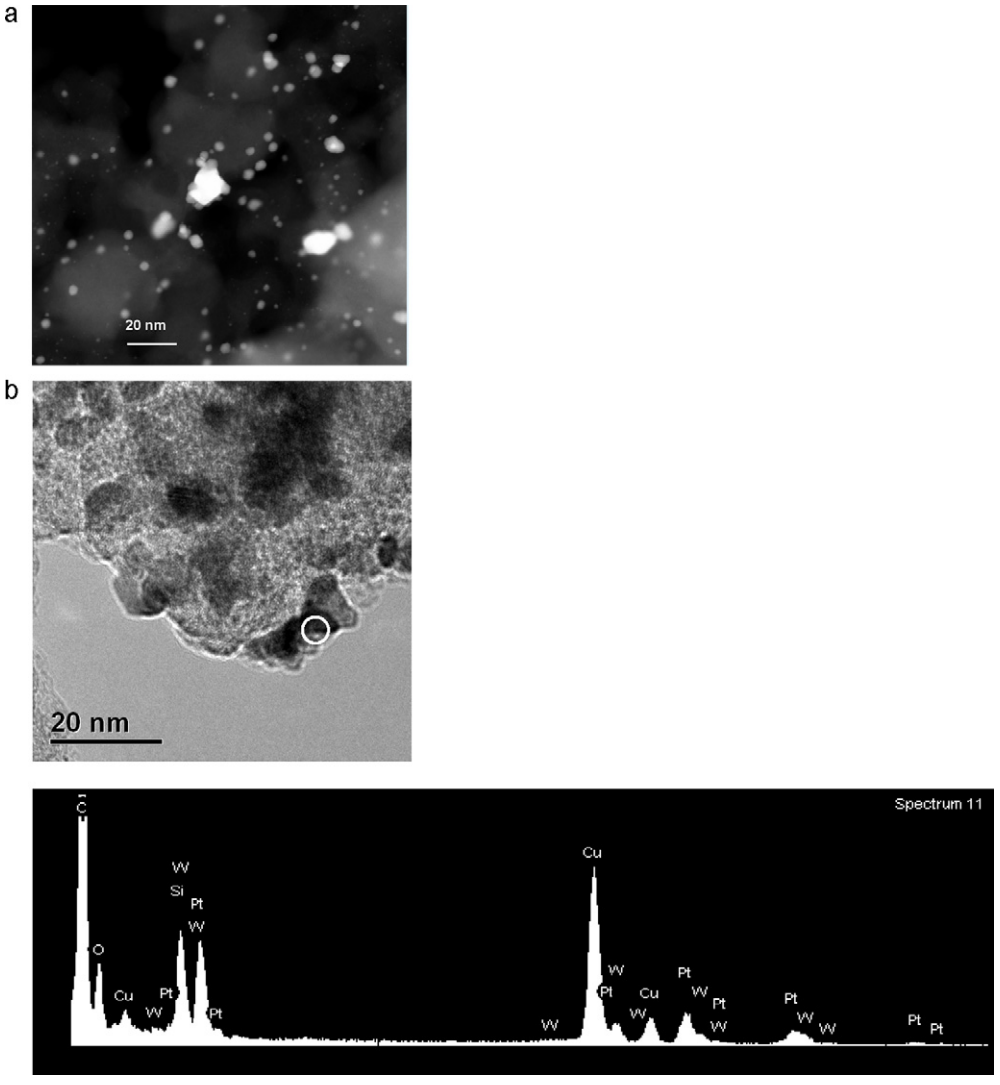

Fig. 6. (a) Low magnification TEM image of Pt/WCctabr catalyst. (b) HREM spectrum for Pt/WCctabr catalyst.

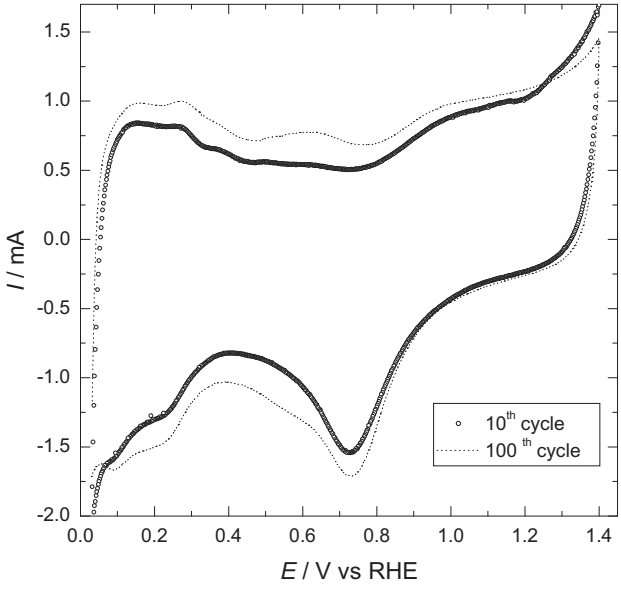

Fig. 8. Cyclic voltammograms recorded after repetitive cycling, at Pt/WCctabr RDE in 0.5 mol dm^{-3} $HClO_4$, at 25 °C with sweep rate of 100 mV s^{-1}.

The polarization curves for oxygen reduction reaction at synthesized Pt/C, Pt/WC_{WO_3} and Pt/WCctabr catalysts obtained at rotation rate of 3405 rpm, in O_2 saturated 0.5 mol dm^{-3} $HClO_4$ solution are presented in Fig. 10.

As an electrochemical reaction that takes place under mixed control, the measured current density for oxygen reduction would be expressed by following equation:

$$\frac{1}{j} = \frac{1}{j_k} + \frac{1}{B\omega^{1/2}} \quad (1)$$

where: j_k is activation controlled (kinetic) current density and $B\omega^{1/2}$ is diffusion-limited current density that is a linear function of the square root of the rotation rate. It could be seen that at all catalysts almost the same diffusion limiting current density (expressed per geometric surface area) at the constant rotation rate was achieved (about 10% discrepancy is within acceptable

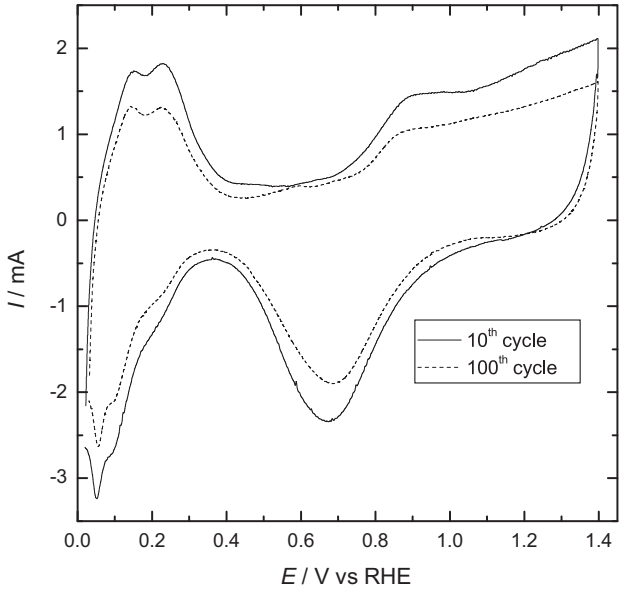

Fig. 9. Cyclic voltammograms recorded after repetitive cycling, at Pt/C RDE in 0.5 mol dm^{-3} $HClO_4$, at 25 °C with sweep rate of 100 mV s^{-1}.

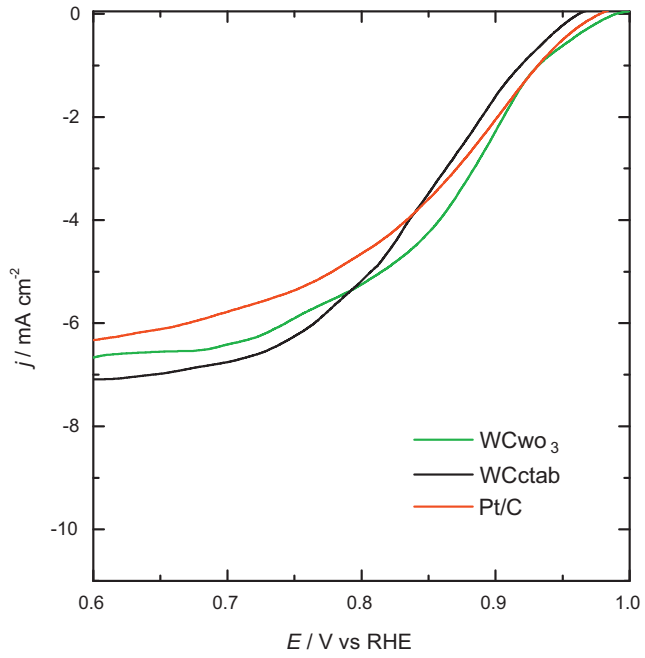

Fig. 10. Polarization curves for ORR at Pt/C, Pt/WC_{WO_3} and Pt/WCctabr catalysts, in 0.5 mol dm^{-3} $HClO_4$ solution, at 3040 rpm rotation rate, sweep rate 20 mV s^{-1}. Current densities are normalized to the geometric surface area.

experimental error). In order to compare catalytic activities in terms of kinetic current densities (per electrochemically active surface area) and mass activities at the constant potential, the Tafel plots have been presented. Kinetic currents, presented as $E - \log j_k$ dependence in Fig. 11, have been determined from Eq. (1).

Tafel plots, presenting potential–kinetic current densities dependences, for oxygen reduction reaction at all investigated catalysts, in 0.5 mol dm^{-3} $HClO_4$ have been presented in Fig. 11. Two different Tafel slopes were obtained for all catalysts, one close to 60 mV dec^{-1} in low current densities region, and other close to 120 mV dec^{-1} in high current densities region, as it is well known for oxygen reduction reaction at Pt based catalysts in acid solution. The differences in catalytic activity between the catalysts are obvious. Better catalytic activities of Pt nanocatalysts on tungsten based

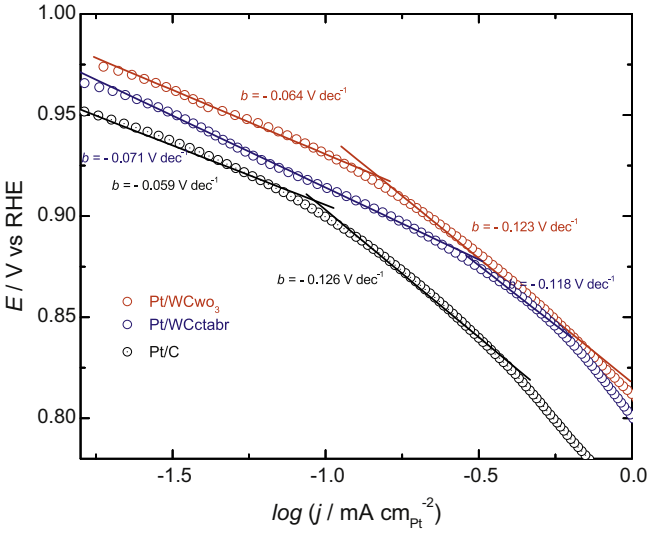

Fig. 11. Tafel plots for ORR in 0.5 mol dm^{-3} $HClO_4$, at Pt/C, Pt/WC_{WO_3} and Pt/WCctabr catalysts, at 25 °C.

supports have been observed. The best catalytic activity, expressed in terms of kinetic current per real surface area of Pt, exhibited Pt/WC_{WO_3}. Increase of the catalytic activity could be explained through synergetic effect between Pt and support. Namely, a shift to higher potentials of the platinum oxide reduction peak was observed for Pt/WC_{WO_3} (0.75 V vs RHE, Fig. 7) compared to Pt/C (0.68 V vs RHE, Fig. 9). Such anodic shift could be attributed to a decrease in the desorption free energy (ΔG_{ads}) of Pt—OH and Pt—O, meaning that the adsorption strength of oxygen containing species on Pt/WC_{WO_3} catalyst is lower than on Pt/C, so, the reduction of intermediates containing oxygen is more facile [15]. Specific and mass activities at the constant potential, of these catalysts have been compared with Pt/C in Table 1. In the same table catalytic activities for different Pt catalyst on tungsten based supports, reported in the literature, have been presented. The presented results showed remarkable enhancement in the ORR kinetics of these novel catalysts, especially Pt/WC_{WO_3}, compared with Pt/C, as well as with already reported catalytic activity values for Pt catalysts on tungsten based supports.

4. Conclusion

Platinum based catalysts on tungsten based supports have been synthesized and characterized as cathode for PEMFCs. Home made supports – WC_{WO_3} and WCctabr, have been characterized by BET, XRD and TEM techniques. Determined specific surface area was 175 $m^2\ g^{-1}$ and 80 $m^2\ g^{-1}$, respectively. XRD analysis revealed presence mainly W corresponding peaks.

Core/shell structure for WCctabr support – W core and WC shell onto it, with thickness between 1 and 5 nm was proved by STEM and EELS techniques. Bimodal platinum size distribution has been found by STEM technique.

The best catalytic activity for oxygen reduction in acid solution and stability after repetitive cycling tests, exhibited Pt/WC_{WO_3} catalyst. Increase in catalytic activity was attributed to synergetic effect between platinum and support.

Acknowledgments

This work was financially supported by the Ministry of Education and Science, Republic of Serbia, under Contract No. 172054.

Electron microscopy characterization was performed at the National Center for Electron Microscopy, which is supported by the Office of Science, Office of Basic Energy Sciences, of the U.S. Department of Energy under Contract No. DE-AC02-05CH11231.

References

[1] A. Morozan, B. Jousselme, S. Palacin, Energy & Environmental Science 4 (2011) 1238–1254.
[2] U.A. Paulus, T.J. Schmidt, H.A. Gaisteiger, R.J. Behm, Journal of Electroanalytical Chemistry 495 (2001) 134–145.
[3] F. Maillard, M. Martin, F. Gloaguen, J.M. Leger, Electrochimica Acta 47 (2002) 3431–3440.
[4] R. Benitez, A.M. Chaparro, L. Daza, Journal of Power Sources 151 (2005) 2–10.
[5] Q. Huang, H. Yang, Y. Tang, T. Lu, D.L. Akins, Electrochemistry Communications 8 (2006) 1220–1224.
[6] Z. Liu, Z.Q. Tian, S.P. Jiang, Electrochimica Acta 52 (2006) 1213–1220.
[7] M. Mathias, R. Makharia, H. Gasteiger, J. Conley, T. Fuller, C. Gittleman, S. Kocha, D. Miller, C. Mittesteadt, T. Xie, S. Yan, P. Yu, Interface 14 (2005) 24–35.
[8] H. Chhina, S. Campbell, O. Kesler, Journal of Power Sources 164 (2007) 431–440.
[9] C.A. Reiser, L. Bregoli, T.W. Patterson, S. Yi Jung, J.D. Yang, M.L. Perry, T.D. Jarvi, Electrochemical and Solid-State Letters 8 (2005) A273–A276.
[10] Y. Shao, G. Yin, Y. Gao, Journal of Power Sources 171 (2007) 558–566.
[11] H.H. Hwu, J.G. Chen, Journal of Physical Chemistry B 107 (2003) 2029–2039.
[12] D.V. Esposito, J.G. Chen, Energy & Environmental Science, http://dx.doi.org/10.1039/c1ee01851e.
[13] M.C. Weidman, D.V. Esposito, I.J. Hsu, J.G. Chen, Journal of the Electrochemical Society 157 (2010) F179–F188.
[14] Q. Zhu, S. Zhou, X. Wang, S. Dai, Journal of Power Sources 193 (2009) 495–500.
[15] L.G.R.A. Santos, K.S. Freitas, E.A. Ticianelli, Journal of Solid State Electrochemistry 11 (2007) 1541–1548.
[16] Z. Shengsheng, Z. Hong, Y. Hongmei, H. Junbo, Y. Baolian, M. Pingwen, Chinese Journal of Catalysis 28 (2007) 109–111.
[17] Y. Wang, S. Song, V. Maragou, P.K. Shen, P. Tsiakaras, Applied Catalysis B: Environmental 89 (2009) 223–228.
[18] P.K. Shen, S. Yin, Z. Li, C. Chen, Electrochimica Acta 55 (2010) 7969–7974.
[19] M.K. Jeon, K.R. Lee, W.S. Lee, H. Daimon, A. Nakahara, S.I. Woo, Journal of Power Sources 185 (2008) 927–931.
[20] E. Antolini, E.R. Gonzalez, Applied Catalysis B: Environmental 96 (2010) 245–266.
[21] H. Meng, P.K. Shen, Z. Wei, S.P. Jiang, Electrochemical and Solid-State Letters 9 (7) (2006) A368–A372.
[22] C. Liang, L. Ding, C. Li, M. Pang, D. Su, W. Li, Y. Wang, Energy & Environmental Science 3 (2010) 1121–1127.
[23] M. Shao, B. Merzougui, K. Shoemaker, L. Stolar, L. Protsailo, Z.J. Mellinger, I.J. Hsu, J. Chen, Journal of Power Sources 196 (2011) 7426–7434.
[24] I.J. Hsu, D.A. Hansgen, B.E. McCandless, B.G. Willis, J. Chen, The Journal of Physical Chemistry C 115 (2011) 3709–3715.
[25] R. Ganesan, D.J. Ham, J.S. Lee, Electrochemistry Communications 9 (2007) 2576–2579.
[26] K.W. Park, K.S. Seul, Electrochemistry Communications 9 (2007) 2256–2260.
[27] B.M. Babic, Lj.M. Vracar, V. Radmilovic, N.V. Krstajic, Electrochimica Acta 51 (2006) 3820–3826.
[28] K.J.J. Mayrhofer, D. Strmcnik, B.B. Blizanac, V. Stamenkovic, M. Arenz, N.M. Markovic, Electrochimica Acta 53 (2008) 3181–3188.
[29] H. Chhina, S. Campbell, O. Kesler, Journal of Power Sources 179 (2008) 50–59.